Eur. Phys. J. B **79**, 107–113 (2011)
DOI: 10.1140/epjb/e2010-10700-1

THE EUROPEAN PHYSICAL JOURNAL B

Regular Article

Homogeneous bubble nucleation limit of mercury under the normal working conditions of the planned European spallation neutron source

A.R. Imre[1], A.S. Abyzov[2,3], I.F. Barna[1,a], and J.W.P. Schmelzer[3,4]

[1] KFKI Atomic Energy Research Institute, 1525 Budapest, POB 49, Hungary
[2] National Science Center, Kharkov Institute of Physics and Technology, Academician Str. 1, 61108 Kharkov, Ukraine
[3] Bogoliubov Laboratory of Theoretical Physics, Joint Institute for Nuclear Research, ul. Joliot-Curie 6, 141980 Dubna, Russia
[4] Institut für Physik der Universität Rostock, Wismarsche Str. 43-45, 18051 Rostock, Germany

Received 13 September 2010 / Received in final form 3 November 2010
Published online 21 December 2010 –

Abstract. In spallation neutron sources, liquid mercury, upon adsorbing the proton beam, is exhibited to large thermal and pressure shocks. These local changes in the state of mercury can cause the formation of unstable bubbles in the liquid, which can damage at their collapse the enclosing the liquid solid material. While there are methods to deal with the pressure shock, the local temperature shock cannot be avoided. In our paper we calculated the work of the critical cluster formation (for mercury micro-bubbles) together with the rate of their formation (nucleation rate). It is shown that the homogeneous nucleation rates are very low at the considered process conditions even after adsorbing several proton pulses, therefore, the probability of temperature induced homogeneous bubble nucleation is negligible.

1 Introduction

Irradiating liquid metals (usually mercury) with proton beams is one of the best known methods to produce high-intensity, multi-purpose neutron beams. This method has been used in various existing facilities and it is planned to be employed in the European spallation source (ESS), too. Unfortunately upon adsorbing the high-intensity proton beam in the liquid the neutrons are not the only particles emitted; an unavoidable heat and pressure wave will be emitted simultaneously from the adsorption region. The increase of the temperature and (in the negative period of the pressure wave) the decrease of the pressure can cause cavitation in the liquid. The metal vapor bubbles then will flow with the liquid and upon reaching high pressure and low temperature regions, they will collapse, causing eventually some severe damage in nearby solid structures. This phenomenon is known as cavitation erosion and one of the main factors which (due to pitting and weight loss) significantly may shorten the lifetime of structural materials. To our present knowledge, four mercury targets are needed at the Oak Ridge spallation neutron source (SNS) at 1 mW power per year. Therefore to avoid cavitation is one of the main challenges of the design of the spallation source target [1–7].

It should be mentioned here that, along the methods to minimize cavitation itself, there are two other ways to minimize the damage. One of them consist in the various ways of surface treatments (plasma nitriding, plasma carbonizing, etc.), which makes the surface more resistant to the damaging pressure wave emitted by the collapsing bubble [8,9]. The other one is the addition of helium micro-bubbles, which is a proven way to soften up and to reduce the damage by absorbing the expansion of liquid mercury and mitigating the pressure waves [8–12]. Considering this method as a successful one to deal with the pressure-drop induced cavitation, in our paper we focused our attention mainly on the temperature increase induced cavitation and allowed only small pressure changes to occur (down to −5 bar).

Our main aim is to find out whether the conditions discussed here are able to cause cavitation or not. We approached the problem in three steps. In the first step (Sect. 2), we calculated the phase equilibrium properties, the stability limit and various other properties of mercury by using a slightly modified version of the equation of state proposed by Redlich and Kwong [13], Morita et al. [14–16]. In the next step (Sect. 3), we made an estimation for the magnitude of pressure and temperature changes by using single and repeated proton pulses. In the final step (Sect. 4), we calculated the work of critical bubble formation in mercury as well as the rate of homogeneous nucleation in the pressure-temperature range defined according to the results of the previous section. The paper is completed by a short summary and discussion (Sect. 5).

[a] e-mail: barnai@aeki.kfki.hu

2 Model system

2.1 Location of binodal and spinodal curves

For the description of mercury (Hg) in both the liquid and gas phases, we will apply a slightly modified Redlich-Kwong-type equation of state as proposed by Morita et al. (see [13,14] and, in particular, Eq. (15) in [15]). It reads

$$p = \frac{RT}{K(T)(v-b)} - \frac{a(T)}{v(v+c)}, \tag{1}$$

$$a(T) = a_{\mathrm{c}} \left(\frac{T}{T_{\mathrm{c}}}\right)^{n} \qquad \text{at} \qquad T \le T_{\mathrm{c}}, \tag{2}$$

where $R = 8.314\ \mathrm{J\,mol^{-1}}$ is the universal gas constant, p is pressure, v is molar volume, T is temperature, a_{c}, b, c and n are the model parameters specific for the substance, T_{c} is critical temperature. The correction coefficient $K(T)$ is dependent on temperature only, it was introduced in the repulsive term instead of the parameter x_{d}, which is a function of T and p (see [16], in such case Eq. (1) becomes an equation for definition of $p(v,T)$, and has no analytical solution).

We employ further dimensionless variables

$$\Pi = \frac{p}{p_c}, \qquad \omega = \frac{v}{v_c}, \qquad \theta = \frac{T}{T_c}, \tag{3}$$

where v_c is the molar volume, p_c the pressure both at the critical point with the critical temperature, T_c. These parameters can be determined from equation (1) in the common way via

$$\left(\frac{\partial p}{\partial v}\right)_T = \left(\frac{\partial^2 p}{\partial v^2}\right)_T = 0 \qquad \text{at} \qquad T = T_c. \tag{4}$$

The equation of state in reduced variables is given by

$$\Pi(\theta,\omega) = \frac{\theta}{\chi_c(\theta)(\omega-\beta)} - \frac{\alpha(\theta)}{\omega(\omega+\delta)}. \tag{5}$$

Here

$$\chi_c(\theta) = \frac{p_c v_c}{RT_c} K(\theta) \tag{6}$$

is the reduced critical compressibility, and

$$K(\theta) = 1.106697 - 0.106697 \exp\left(\frac{\theta - 1}{0.17026}\right), \tag{7}$$

$$\alpha(\theta) = \frac{a_{\mathrm{c}}\theta^n}{p_c v_c^2} = \alpha\theta^n, \qquad \beta = \frac{b}{v_c}, \qquad \xi = \frac{c}{v_c}. \tag{8}$$

According to [15] we have then

$$\begin{aligned} &\alpha = 2.5272, \quad \beta = 0.3952, \quad \xi = -0.16567, \\ &n = -0.0284127. \end{aligned} \tag{9}$$

From equations (1) and (4) we get [15]

$$\begin{aligned} &v_c = 1.797 \times 10^{-4}\ \mathrm{m^3/kg}, \quad \rho_c = 5566\ \mathrm{kg/m^3}, \\ &p_c = 158 \times 10^6\ \mathrm{Pa}, \qquad T_c = 1762\ \mathrm{K}. \end{aligned} \tag{10}$$

The location of the classical spinodal curve can be found by the determination of the extrema of the thermal equation of state, $\Pi(\theta,\omega)$ (Eq. (5)), considering the temperature θ as constant. By taking the derivative of $\Pi(\theta,\omega)$ with respect to ω, we obtain from equation (5) the result

$$\frac{\partial}{\partial\omega}\Pi(\theta,\omega) = \frac{\alpha(\theta)(2\omega+\xi)}{\omega^2(\omega+\xi)^2} - \frac{\theta}{\chi_c(\omega-\beta)^2} = 0. \tag{11}$$

For $\theta < 1$, this equation has two positive solutions $\omega_{\mathrm{sp}}^{(\mathrm{left})}$ and $\omega_{\mathrm{sp}}^{(\mathrm{right})}$ for ω corresponding to the specific volumes of the both macrophases at the spinodal curves (or at the limits of metastability).

Similarly, the binodal curves give the values of the specific volumes of the liquid and the gas phases coexisting in thermal equilibrium at a planar interface. From the left branch of the binodal curve, we get the specific volume of the liquid phase ($\omega_l^{(\mathrm{eq})}(\theta) = \omega_{\mathrm{b}}^{(\mathrm{left})}(\theta)$), from the right branch of the binodal curve, we obtain the specific volume of the gas ($\omega_g^{(\mathrm{eq})}(\theta) = \omega_{\mathrm{b}}^{(\mathrm{right})}(\theta)$). For $\theta = 1$, both solutions coincide in the critical point ($\omega_l^{(\mathrm{eq})} = \omega_g^{(\mathrm{eq})} = \omega_c = 1$), again. Consequently, in order to determine the specific volumes of the liquid and the gas at some given temperature in the range $\theta \le 1$, we have to specify the location of the binodal curve.

The location of the binodal curve may be determined from the necessary thermodynamic equilibrium conditions (for planar interfaces) – equality of pressure and chemical potentials – via the solution of the set of equations

$$\Pi_l(\omega_l,\theta) = \Pi_g(\omega_g,\theta), \qquad \mu_l(\omega_l,\theta) = \mu_g(\omega_g,\theta). \tag{12}$$

Here by μ the chemical potential of the atoms or molecules in the liquid (l) and the gas (g) are denoted. Having the equation for the reduced pressure (cf. Eq. (5)), we have now to determine in addition the chemical potential in dependence on pressure and temperature (see Sect. 2.2).

Isotherms for mercury (Eq. (5)) for different values of the reduced temperature $\theta = 0.4$, 0.65, 0.8, 0.891 and 0.92 are shown in Figure 1, dashed and dashed-dotted curves present the binodal and spinodal curves, correspondingly. One can see, that there are two classes of isotherms: for the first one (when $\theta \ge \theta_s$), the pressure is always positive, i.e. $p \ge 0$, while for the second class (at $\theta < \theta_s$) pressure may be both positive and negative. The parameter θ_s is determined via the equation

$$\Pi_l(\omega_{\mathrm{sp}}(\theta_s),\theta_s) = 0. \tag{13}$$

For mercury, it has the value $\theta_s \approx 0.891$ and $T_s \equiv T_c\theta_s \approx 1570$ K. A comparison of experimental data [17,18] for the vapor-liquid coexistence properties of mercury with results obtained in this work are shown in Figures 2 and 3 in (T,ρ) and (p,T^{-1})-variables, respectively.

2.2 Determination of the chemical potential and the interfacial tension

For isothermal processes, the change of the Helmholtz free energy, F, may be expressed as

$$dF = -pdV + \mu dn. \tag{14}$$

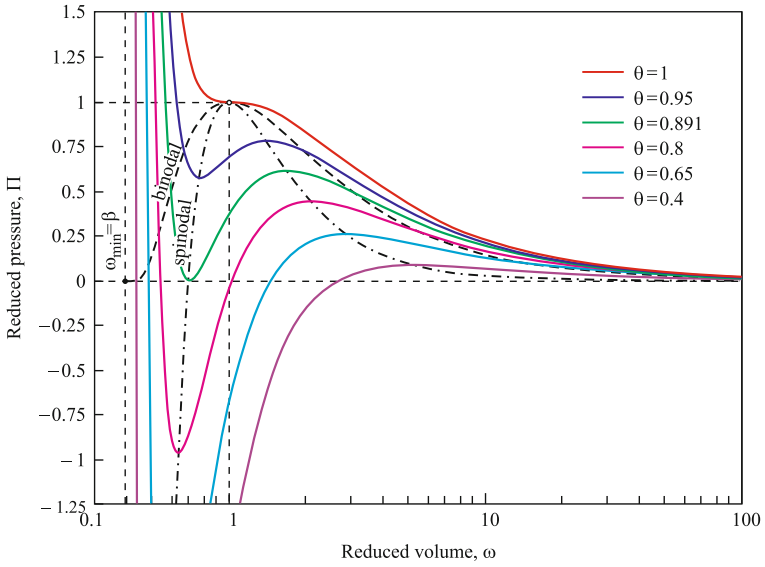

Fig. 1. (Color online) Isotherms of mercury as described via equation (5) for different values of the reduced temperature, from $\theta = 0.4$ (bottom curve) to $\theta = 1$ (upper curve).

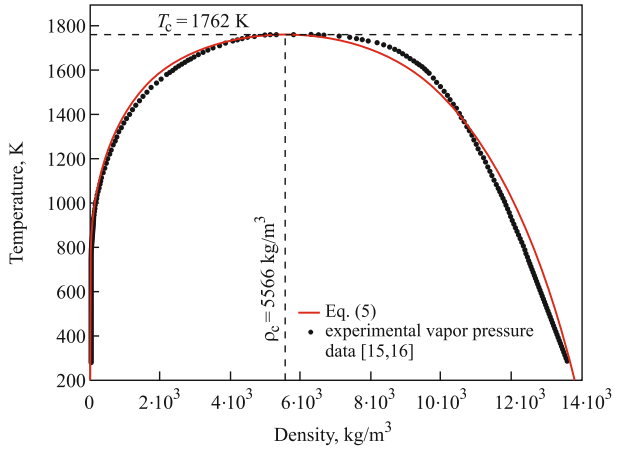

Fig. 2. (Color online) Comparison of experimental data (according to [17,18]) for the vapor-liquid coexistence properties of mercury with the theoretical results (full curve determined via Eq. (5)) obtained in this work.

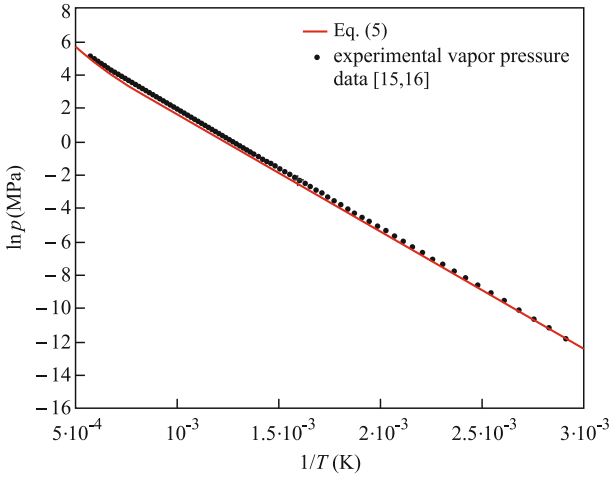

Fig. 3. (Color online) Comparison of experimental vapor pressure for mercury (according to [17,18]) with theoretical results (full curve determined via Eq. (5)) obtained in this work.

Here V is the volume of the system and n the number of moles in it. For a given fixed mole number, n, of the substance ($n = \text{const.}$), we have,

$$d\varphi_n = -pdv, \quad \varphi_n = \frac{F}{n}, \quad v = \frac{V}{n}, \tag{15}$$

or, in reduced variables,

$$d\left(\frac{\varphi_n}{p_c v_c}\right) = -\Pi d\omega. \tag{16}$$

Combining equation (16) with the equation of the state, equation (5), we obtain

$$\left(\frac{\varphi_n}{p_c v_c}\right) = -\left[\frac{\alpha(\theta)}{\xi}\ln\left(1+\frac{\xi}{\omega}\right) + \frac{\theta}{\chi_c(\theta)}\ln(\omega-\beta)\right]. \tag{17}$$

Alternatively, the isochoric change of the Helmholtz free energy is given at constant temperature by

$$dF = \mu dn. \tag{18}$$

From equation (18),

$$d\varphi_v = -\frac{\mu}{v^2}dv, \qquad \varphi_v = \frac{F}{V}. \tag{19}$$

On the other side, the functions φ_v and φ_n are connected by

$$F = \varphi_n n = \varphi_v V, \qquad \varphi_v = \frac{\varphi_n}{v}. \tag{20}$$

With equation (17), we have then

$$\varphi_v = \frac{p_c}{\omega}\left[\frac{\alpha(\theta)}{\xi}\ln\left(1+\frac{\xi}{\omega}\right) + \frac{\theta}{\chi_c(\theta)}\ln(\omega-\beta)\right]. \tag{21}$$

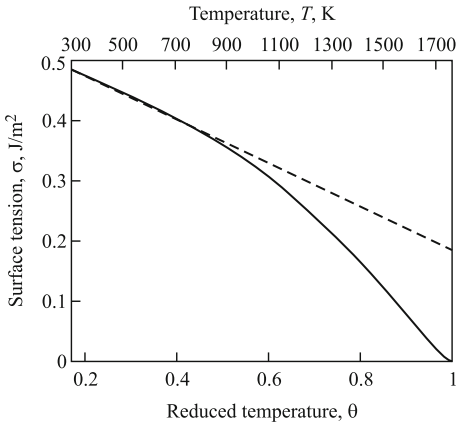

Fig. 4. Dependence of the surface tension on temperature, solid curve presents equation (24) at $\omega_{\rm l} = \omega_{\rm b}^{(\rm left)}$, $\omega_{\rm g} = \omega_{\rm b}^{(\rm right)}$, and dashed curve – equation (26).

With equations (19) and (21), the expression for the chemical potential of a heavy liquid metal (HLM) can be obtained then via

$$\mu = -v^2 \frac{\partial \varphi_v}{\partial v} = -v_c \omega^2 \frac{\partial \varphi_v}{\partial \omega}. \tag{22}$$

This relation yields

$$\frac{\mu}{p_c v_c} = -\left[\frac{\alpha(\theta)}{\omega + \xi} + \frac{\theta\omega}{\chi_c(\theta)(\omega - \beta)} + \frac{\alpha(\theta)}{\xi} \ln\left(1 + \frac{\xi}{\omega}\right) + \frac{\theta}{\chi_c(\theta)} \ln(\omega - \beta)\right]. \tag{23}$$

In addition to the bulk properties of the system, we have to know the value of σ (surface tension) for planar interfaces in dependence on the parameters describing the state of both phases. The following form was chosen for our calculation [19–22]

$$\sigma\left(\omega_{\rm g}, \omega_{\rm l}, \theta\right) = \Theta(\theta) \left[\frac{1}{\omega_{\rm l}} - \frac{1}{\omega_{\rm g}}\right]^{\delta}, \qquad \delta = 2.5, \tag{24}$$

where

$$\Theta(\theta) = A \left[\frac{1}{\omega_{\rm b}^{(\rm left)}} - \frac{1}{\omega_{\rm b}^{(\rm right)}}\right]^{n-\delta}, \tag{25}$$

and A and n are constant parameters. Comparison of equations (24) and (25) with experimental data [23]

$$\sigma(T) = 0.5446544 - 0.000204917T \tag{26}$$

(valid in this form only for temperatures far below the critical temperature; here the temperature is given in Kelvin and the surface tension in J/m^2) at $\omega_{\rm l} = \omega_{\rm b}^{(\rm left)}$ and $\omega_{\rm g} = \omega_{\rm b}^{(\rm right)}$ yields

$$A = 0.033253 \text{ J/m}^2, \qquad n = 3. \tag{27}$$

In Figure 4, the dependence of the surface tension on temperature is shown, the solid curve presents the results obtained via equation (24) at $\omega_{\rm l} = \omega_{\rm b}^{(\rm left)}$, $\omega_{\rm g} = \omega_{\rm b}^{(\rm right)}$, and dashed curve corresponds to equation (26).

3 Determination of the pressure and temperature change after proton adsorption

For the determination of the pressure and temperature change, a "one dimensional six-equation two-fluid model" was employed, which is capable to describe transient-like pressure waves and quick evaporation or condensation which is proportional to cavitation caused by energetic proton interaction in mercury target [24]. The method was developed to describe the sudden and drastic steam condensation, called water hammer [25,26].

The model contains six first-order partial-differential equations which describe one-dimensional surface-averaged mass, momentum and energy conservation laws for both phases. A special numerical procedure ensures that shock-waves can be described without any numerical dispersion. With two major modifications this model can be applied to investigate the thermo-hydraulic properties of the planned mercury target in the european spallation source (ESS). These modifications are the following: the equation of state namely the density and the internal energy of both mercury phases should be known in a broad range of pressure (1 Pa to 100 MPa) and temperature (273 K to 1000 K). As a second point the interaction of the high energy proton beam with mercury has to be included. This is a much simpler task because we may consider that about 50% of the 300 kJ/pulse beam energy is absorbed as a 2 ms long heat shock square pulse, giving a new source term in the energy equation of the liquid phase. The ESS mercury target station is modeled as a 18 m long closed loop which is bent in three dimensions and the pipe diameter is 15 cm. We consider that 150 kJ heat is absorbed in a 10 cm long pipe, this is approximately the width of the proton pulse. Calculation shows that such a single pulse heats up the mercury with about 40−44 K, assuming that the initial temperature was between 293−373 K (i.e. within the normal working range of the spallation source). In the calculations, low velocities 0.5−4 m/s, low initial pressure 1−4 bar and low initial temperature (below 374 K) were assumed. To our knowledge the existing Japanese Spallation Neutron Source Hg loop is about 15 m long, with a diameter of 15 cm, the flow velocity of Hg is 0.7 m/s and the pressure is approximately equal to 1 bar.

Concerning the pressure change, the model is able to estimate the positive part, but at the negative region (where most of the low temperature cavitation is expected to happen [27]), a stability problem aroused. Therefore we focused our calculation to the heat shock and, at present, neglected the pressure change. Preliminary calculation yielded a few bar changes [24], in agreement with the results of Ida [28], therefore the latter calculations were performed in the −5 to 10 bar range. We should mention here, that other models predicted much larger pressure changes (even hundreds of bars) [29,30] both in the positive and negative pressure region.

Also the effects of repeated pulses were checked. The calculations were performed with a 2 ms square pulse train

where the delay time was 20 ms which is similar to a 16 Hz repetition rate. We started with a flow system with initial $p = 4$ bar, $T_{initial} = 353$ K and initial flow velocity $v = 4$ m/s. We found that the temperature jumps are more or less additive which means that after the beginning of the third pulse the temperature was about 430 K.

4 Determination of the work of critical cluster formation

Let us assume that the system is brought suddenly into a metastable state located between binodal curve and spinodal curve on the liquid side. Then, by nucleation and growth processes, bubbles may appear spontaneously in the liquid and a phase separation takes place [31]. Based on the relations outlined above, we will determine now the temperature and pressure dependence of the parameters of the critical vapour cluster formation.

We start with the general expression for the change of the thermodynamic potential

$$\Delta G = \sigma A + (p - p_\alpha) V_\alpha + \sum_j n_{j\alpha} \left[\mu_{j\alpha} - \mu_{j\beta}\right]. \quad (28)$$

Here the subscript α specifies the parameters of the cluster (bubble) phase while β refers to the ambient liquid phase. This relation holds as long as the state of the liquid remains unchanged by the formation of one bubble. For a one-component system, this expression is reduced to

$$\Delta G = \sigma A + (p - p_\alpha) V_\alpha + n_\alpha \left[\mu_\alpha - \mu_\beta\right]. \quad (29)$$

As independent variables, we selected the radius of the bubble, r, and the molar volume of the gas phase in the bubble. Similarly to [19,32,33], we arrive then at

$$\frac{\Delta g\left(r, \omega_\mathrm{g}, \omega_\mathrm{l}, \theta\right)}{k_\mathrm{B} T} = 3\left(\frac{1}{\omega_\mathrm{l}} - \frac{1}{\omega_\mathrm{g}}\right)^\delta r^2 + 2 f\left(\omega_\mathrm{g}, \omega_\mathrm{l}, \theta\right) r^3, \quad (30)$$

where the following notations have been introduced:

$$f\left(\omega_\mathrm{g}, \omega_\mathrm{l}, \theta\right) = \Pi\left(\omega_\mathrm{g}, \theta\right) - \Pi\left(\omega_\mathrm{l}, \theta\right) + \frac{1}{\omega_\mathrm{g}} \times \left(\frac{\mu\left(\omega_\mathrm{l}, \theta\right) - \mu\left(\omega_\mathrm{g}, \theta\right)}{p_c v_c}\right), \quad (31)$$

$$g \equiv \frac{G}{\Omega_1}, \qquad \Omega_1 = \frac{16\pi}{3} \frac{1}{p_c^2 k_\mathrm{B} T_c \theta} \Theta(\theta)^3, \quad (32)$$

$$r \equiv \frac{R}{R_\sigma}, \qquad R_\sigma = \frac{2}{p_c} \Theta(\theta). \quad (33)$$

The dependence of the scaling parameters Ω_1 and R_σ on the reduced temperature is shown in Figure 5.

The Gibbs free energy surface for the metastable initial state has a typical saddle shape near to the configuration corresponding to a bubble of critical size (see Fig. 6, $\theta = 0.92$, $\omega_\mathrm{l} = 0.65$) in the space of critical radius-molar volume and work of cluster formation. The critical point position is determined by the following set of equations

$$\frac{\partial \Delta g\left(r, \omega_\mathrm{g}, \omega_\mathrm{l}, \theta\right)}{\partial r} = 0, \qquad \frac{\partial \Delta g\left(r, \omega_\mathrm{g}, \omega_\mathrm{l}, \theta\right)}{\partial \omega_\mathrm{g}} = 0. \quad (34)$$

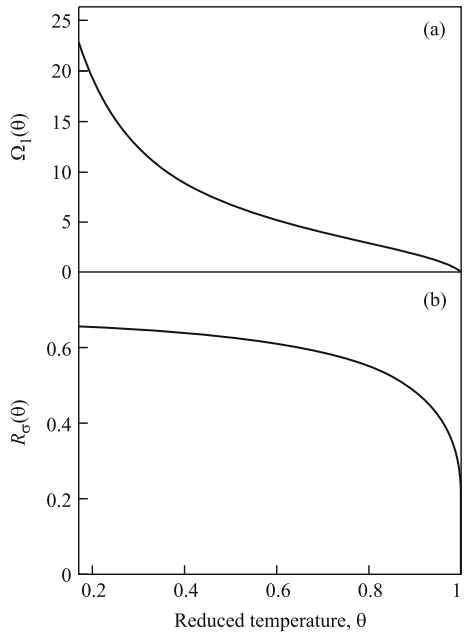

Fig. 5. Dependence of the scaling parameters Ω_1 and R_σ on the reduced temperature, θ.

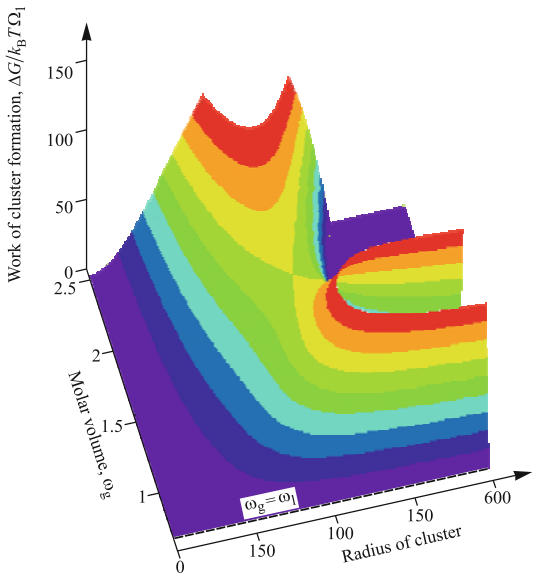

Fig. 6. (Color online) Gibbs free energy surface for metastable initial state, $\theta = 0.92$, $\omega_\mathrm{l} = 0.65$.

The dependence of the critical cluster parameters on the initial molar volume of liquid, ω_l, are shown in Figures 7–9, for different values of temperature, $\theta = 0.17$, 0.5, 0.7, 0.8, 0.891 and 0.92. The positions of the binodal curves are given then by $\omega_\mathrm{b}^{(\mathrm{left})} = 0.409$, 0.45, 0.494, 0.531, 0.589, 0.62, and $\omega_\mathrm{b}^{(\mathrm{right})} = 1.663 \times 10^8$, 90.5, 11.606, 5.634, 3.043, 2.475, the respective parts of the spinodal curves are located at $\omega_\mathrm{sp}^{(\mathrm{left})} = 0.452$, 0.528, 0.59, 0.634, 0.696, 0.726, and $\omega_\mathrm{sp}^{(\mathrm{right})} = 13.609$, 4.04, 2.584, 2.087, 1.679, 1.547, correspondingly.

The dependence of the work of formation and radius of the critical cluster on temperature for the practically

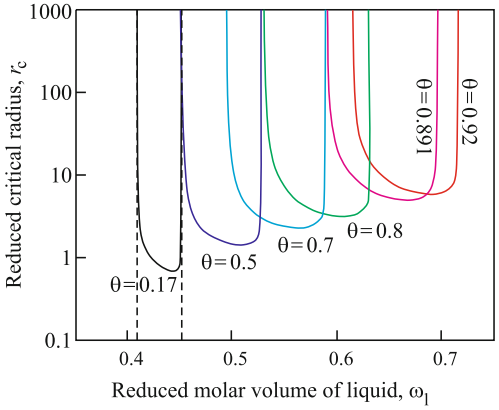

Fig. 7. (Color online) Dependence of the critical cluster radius, $r_c = R_c/R_\sigma$, on the initial molar volume of liquid, ω_l, for different values of temperature, $\theta = 0.17$, 0.5, 0.7, 0.8, 0.891 and 0.92.

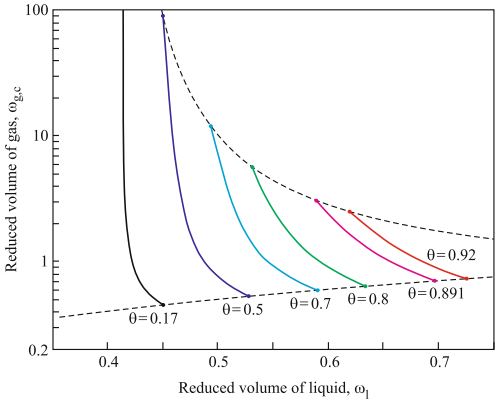

Fig. 8. (Color online) Dependence of the gas molar volume in critical bubble, $\omega_{g,c}$, on the initial molar volume of liquid, ω_l, for different values of temperature, $\theta = 0.17$, 0.5, 0.7, 0.8, 0.891 and 0.92.

significant cases $p = -5, 0, 1, 2, 5$ and 10 bar is presented in Figure 10. In Figure 11, the dependence of the nucleation rates on temperature for the same values of pressure are shown (a value of the pre-exponential factor of $J_0 = 10^{41}$ s^{-1} m^{-3} has been used for the calculations). One can see, that in such case homogeneous nucleation is possible only at very high temperatures, near $T_s \approx 1570$ K. One can observe as well that concerning a 20 cm diameter sphere (region of proton adsorption) and 2 ms time span, one can expect 1 or more nucleation events above 1530.5 K. We arrive in this way at the conclusion that at the conditions analyzed intensive formation of supercritical bubbles by homogeneous nucleation is included. However, heterogeneous nucleation induced by different kinds of nucleation cores dissolved in liquid mercury may occur, of course, also at lower temperatures.

5 Conclusions

In spallation neutron sources, liquid mercury is the subject of large thermal and pressure shocks (including negative

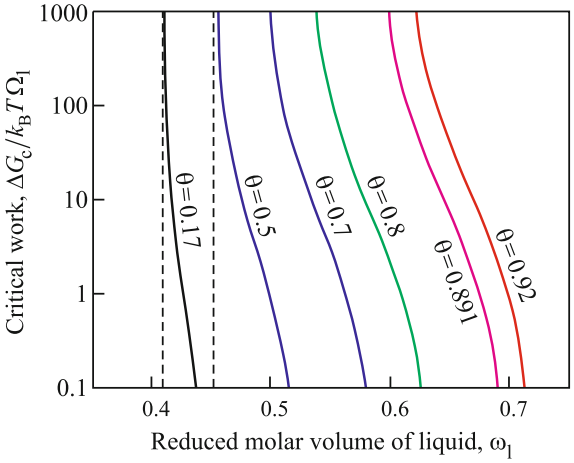

Fig. 9. (Color online) Dependence of the work of critical cluster formation, $\Delta G_c/k_B T\Omega_l$, on the initial molar volume of liquid, ω_l, for different values of temperature, $\theta = 0.17$, 0.5, 0.7, 0.8, 0.891 and 0.92.

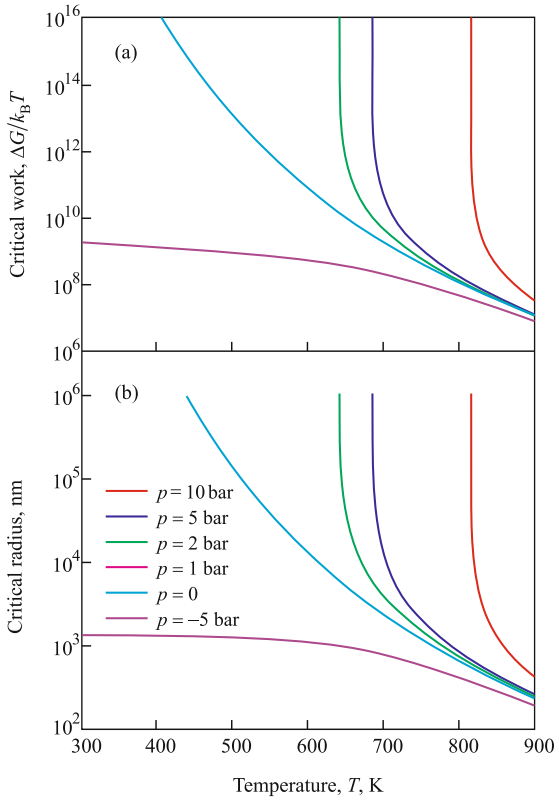

Fig. 10. (Color online) Dependence of the work of critical cluster formation, $\Delta G_c/k_B T$ (a), and of the critical cluster radius (b) on temperature for $p = -5$, 0, 1, 2, 5 and 10 bar.

pressures) upon adsorbing the proton beam. Increased temperature and negative pressure can result in the formation of unstable bubbles which can cause cavitation erosion of the structural material, shortening the life-time of the equipment and contaminating the liquid mercury with tiny steel pieces. Therefore it is crucial to avoid or minimize bubble nucleation. While pressure shock can be softened by adding helium micro-bubbles to the mercury,

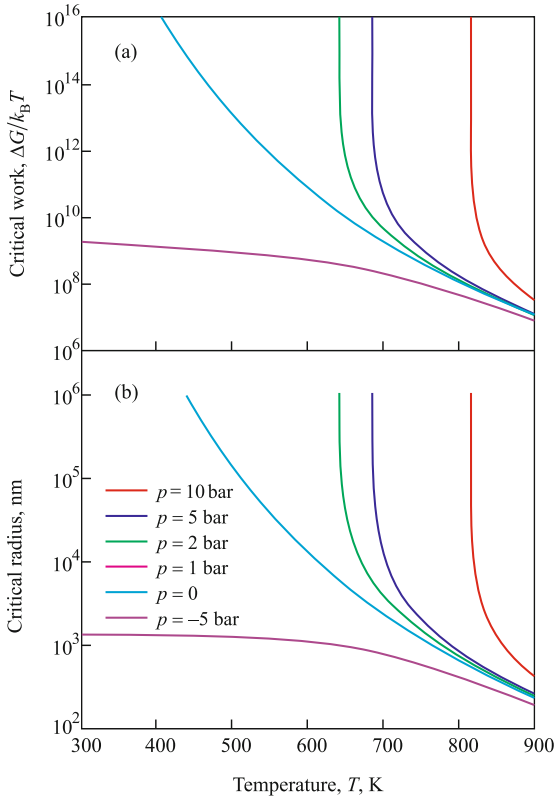

Fig. 11. (Color online) Dependence of the nucleation rate on temperature for $p = -5$, 0, 1, 2, 5 and 10 bar.

there is no way to deal with the thermal shock (i.e. local heating is not possible in the middle of the liquid mercury). Therefore our calculation focused on the calculation of the degree of temperature increase, the work of critical cluster formation (i.e. the nucleus of a macroscopic bubble) and the nucleation rate. It has been shown that after repeated proton pulses the temperature can be increased with a few hundred K, but the nucleation rate is so low that the possibility of homogeneous nucleation (i.e. bubble formation in the pure mercury) is highly improbable, even when the pressure gets values below the vapor pressure.

The authors express their gratitude to the Hungarian Academy of Sciences for financial support in the framework of the common Hungary-Russia/Dubna project EAI-2009/004 and DFFD of Ukraine for partial financial support in the framework of the common Ukraine-Byelorussia project F29.2/019, contract Number FP7 GA n° 202247 "NeutronSourceESS".

References

1. M. Futukawa, H. Kogawa, H. Rino, H. Date, H. Takeshi, Int. J. Impact Eng. **28**, 123 (2003)
2. B.W. Riemer, J.R. Haines, J.D. Hunn, D.C. Lousteau, T.J. McManamy, C.C. Tsai, J. Nucl. Mat. **92**, 318 (2003)
3. H. Date, M. Futakawa, Int. J. Impact Eng. **32**, 118 (2005)
4. N.J. Nicholas, P.V. Chitnis, R.G. Holt, R.A. Roy, R.O. Cleveland, B. Riemer, M. Wendel, J. Acoust. Soc. Am. **127**, 2231 (2010)
5. D.A. McClintock, P.D. Ferguson, L.K. Mansur, J. Nucl. Mat. **398**, 73 (2010)
6. J.R. Haines, B.W. Riemer, D.K. Felde, J.D. Hunn, S.J. Pawel, C.C. Tsai, J. Nucl. Mat. **343**, 58 (2005)
7. S.J. Pawel, L.K. Mansur, J. Nucl. Mat. **398**, 180 (2010)
8. T. Naoe, I. Masato, M. Futukawa, Nucl. Inst. Meth. Phys. Res. A **586**, 382 (2008)
9. T. Naoe, M. Futukawa, T. Shoubu, T. Wakui, H. Kogawa, H. Takeuchi, M. Kawai, J. Nucl. Sci. Technol. **45**, 698 (2008)
10. R.P. Taleyarkhan, F. Moraga, Nucl. Eng. Des. **207**, 181 (2001)
11. M. Futukawa, H.T. Kogawa, S. Hasegawa, T. Naoe, I. Masato, K. Haga, T. Wakui, N. Tanaka, Y. Mashumoto, Y. Ikeda, J. Nucl. Sci. Technol. **45**, 1041 (2008)
12. K. Okita, S. Takagi, Y.T. Matsumoto, JFST **3**, 116 (2008)
13. O. Redlich, J.N.S. Kwong, Chem. Rev. **44**, 233 (1949)
14. K. Morita, W. Maschek, M. Flad, Y. Tobita, H. Yamano, J. Nucl. Sci. Techol. **43**, 526 (2006)
15. K. Morita, V. Sobolev, M. Flad, J. Nucl. Mat. **362**, 227 (2007)
16. K. Morita, E.A. Fischer, Nucl. Eng. Des. **183**, 177 (1998)
17. N.B. Vargaftik, Y.K. Vinogradov, V.S. Yargin, *Handbook of Physical Properties of Liquid and Gases*, 3rd edn. (Begell House, New York, 1996)
18. W. Goetzlaff, doctoral thesis, Philips-Universität Marburg, Germany, 1988
19. J.W.P. Schmelzer, J. Schmelzer Jr., J. Chem. Phys. **114**, 5180 (2001)
20. J.D. van der Waals, Ph. Kohnstamm, *Lehrbuch der Thermodynamik* (Johann-Ambrosius-Barth Verlag, Leipzig und Amsterdam, 1908)
21. K. Binder, *Spinodal Decomposition, in Materials Science and Technology*, edited by R.W. Cahn, P. Haasen, E.J. Kramer (VCH, Weinheim, 1991), Vol. 5, p. 405
22. D.B. Macleod, Trans. Faraday Soc. **19**, 38 (1923)
23. J.J. Jasper, Phys. Chem. Ref. Data **1**, 841 (1972)
24. I.F. Barna, A.R. Imre, L. Rosta, F. Mezei, Eur. Phys. J. B **66**, 419 (2008)
25. I. Tiselj, S. Petelin, Trans. ASME J. Fluids Eng. **120**, 363 (1998)
26. I.F. Barna, A.R. Imre, G. Baranyai, Gy. Ezsöl, Nucl. Eng. Des. **240**, 146 (2010)
27. *Liquids Under Negative Pressure*, edited by A.R. Imre, H.J. Maris, P.R. Williams, NATO Science Series (Kluwer, 2002)
28. M. Ida, T. Naoe, M. Futukawa, Phys. Rev. E **75**, 046304 (2007)
29. B.W. Riemer, J. Nucl. Mat. **343**, 81 (2005)
30. S. Ishikura, H. Kogawa, M. Futakawa, K. Kikuchi, R. Hino, C. Arakawa, J. Nucl. Mat. **318**, 113 (2003)
31. V.P. Skripov, *Metastable Liquids* (Nauka, Moscow, 1972; Wiley, New York, 1974)
32. J.W.P. Schmelzer, J. Schmelzer Jr., Atm. Res. **65**, 303 (2003)
33. A.S. Abyzov, J.W.P. Schmelzer, J. Chem. Phys. **127**, 114504 (2007)